ACS APPLIED MATERIALS & INTERFACES

RESEARCH ARTICLE

www.acsami.org

A Substrate-Integrated and Scalable Templated Approach Based on Rusted Steel for the Fabrication of Polypyrrole Nanotube Arrays

Jesus M. Velazquez,[†] Anil V. Gaikwad,[‡] Tapan K. Rout,[*,‡] Javid Rzayev,[*,†] and Sarbajit Banerjee[*,†]

[†]Department of Chemistry, University at Buffalo, The State University of New York, Buffalo, New York 14260-3000, United States

[‡]R, D & T, Tata Steel Group (Europe), 1760-Ijmuiden, The Netherlands

Supporting Information

ABSTRACT: We report here a facile, generalizable, and entirely scalable approach for the fabrication of vertically aligned arrays of Fe_2O_3/polypyrrole core—shell nanostructures and polypyrrole nanotubes. Our "all electrochemical" approach is based on the fabrication of α-Fe_2O_3 nanowire arrays by the simple heat treatment of commodity low carbon steel substrates, followed by electropolymerization of conformal polypyrrole sheaths around the nanowires. Subsequently, electrochemical etching of the nanowires yields large-area vertically aligned polypyrrole nanotube arrays on the steel substrate. The developed methodology is generalizable to functionalized pyrrole monomers and represents a significant practical advance of relevance to the technological implementation of conjugated polymer nanostructures in electrochromics, electrochemical energy storage, and sensing.

KEYWORDS: electropolymerization, polypyrrole nanotubes, α-Fe_2O_3 nanowires, templated synthesis

1. INTRODUCTION

The mesostructuration of conjugated polymers represents a powerful emerging tool in the arsenal of available methods for manipulation of their fundamental electronic and ionic transport behavior.[1−7] The realization that polymeric nanostructures with reduced dimensions show characteristic anisotropic electronic transport due to increased structuring of polymer chains and extended conjugation lengths,[5,7] while also exhibiting enhanced electroactivity due to diminution of solid-state diffusion path lengths,[2,3] has exercised the imaginations of material chemists, electrochemists, and polymer scientists alike. In particular, there has been a flurry of activity focused on the fabrication of quasi-1D arrays of polymeric nanowires and nanotubes, commonly based on variants of the template synthesis approach.[3,7−11] In parallel, recent frenetic efforts have been devoted to integration of these constructs within sensing, electrochromic, supercapacitative, and secondary Li-ion battery electrode architectures.[2−4] We present here a facile, entirely scalable, and generalizable approach for the fabrication of polypyrrole nanotubes on low carbon steel substrates via a combination of electrochemical deposition and etching processes.

There are significant benefits to be derived from reducing the dimensionality of conjugated polymers. The electronic conductivity of conjugated polymers after all is predicated not just on extended π conjugation, but is also strongly dependent on the oxidation and reduction of polymeric chains with the requisite charge compensation derived from the presence of counterions.[12,13] The mobility of the counterions within the amorphous polymeric matrix determines to a large extent the agility with which the conductivity of the polymeric system is transformed in response to an external stimulus. This mass-transport-limited mobility and electroactivity is consequently enhanced by a reduction of the solid-state diffusion path lengths, such as achieved by scaling polymers to nanoscopic domains.[3,4] The greater surface-to-volume ratios of polymeric nanostructures as compared to thin films and granules also enhance the density of accessible redox-active sites and increase the interfacial contact area for ion exchange with electrolyte or analyte solutions, having clear implications for sensing, electrochromics, and electrocatalysis.[1−4] Polymeric nanostructures are also more likely to retain mechanical integrity without delamination upon prolonged electrochemical cycling because of the more facile relaxation of substrate stresses inevitably generated by the volume changes that accompany ion insertion and extraction. As an example of the tantalizing possibilities available for low-dimensional conjugated polymer structures, the accelerated Faradaic pseudocapacitance kinetics realized for polypyrrole, polyaniline, and PEDOT nanocomposites portend applications in electrochemical double layer capacitors delivering high power and energy densities.[14−16]

Considerable progress has been achieved in finely tuning the dimensions and morphologies of polymeric nanostructures with the underlying synthetic principle typically involving the spatially confined polymerization of monomers within a nanoscopic geometric region defined by assemblies of organic molecules or walls of an inorganic lattice. The aptly designated molecular or macromolecular "soft"[17−22] templates range from being

Received: January 17, 2011
Accepted: March 14, 2011
Published: March 22, 2011

surfactant micelles[18,19] to synthetic lipid assemblies[20] or naturally occurring macromolecules such as heparin[21] and starch.[22] In this context, a distinctive recent approach involves the molecular templating of polypyrrole nanotubes from single-molecule bottlebrush copolymers with degradable polylactide backbones.[23] In contrast, "hard" templates impose the geometries of inorganic pores or cavities upon the incipient polymers. Some more ubiquitous examples of such templates include anodic alumina membranes,[3,5−7] zeolites, track-etched polycarbonate membranes, carbon nanotube arrays,[11] V_2O_5 nanowires, and as recently demonstrated, anodized TiO_2 nanotube arrays.[24−26] In each case polymerization can be induced chemically by the addition of the appropriate initiator or electrochemically via anodic oxidation.[1,2] The latter approach is particularly attractive as a facile means of generating exquisitely structured solid-state polymeric nanostructures on electrode geometries.[1]

It is important to note that each set of synthetic methodologies has its unique set of advantages and drawbacks. The soft template approaches typically do not yield good monodispersity of structure,[23] and although soft templates can be used in conjunction with electropolymerization,[1] these processes are not very amenable to the fabrication of well-aligned arrays of nanostructures desirable for applications in electrochromics, supercapacitors, or Li-ion batteries. In contrast, hard template methods based on membranes with well-defined porosities can provide precise control of nanostructure dimensions and yield well-aligned arrays of polymeric nanostructures but are not scalable to large areas. Indeed, scalability and cost considerations have received scant regard, and represent some of the biggest obstacles to technological implementation of conjugated polymer nanostructures. The distinctive approach we present here uses a facile set of processing steps to fabricate well-defined substrate-integrated polypyrrole nanostructures using α-Fe_2O_3 nanowires grown on steel by a simple oxidation protocol as a template for electropolymerization. The inexpensive precursors and facile processing steps provide a unique scalable methodology for the large-area fabrication of well-aligned polypyrrole nanotube arrays.

The fabrication of iron-oxide/polypyrrole nanocomposites has been variously attempted via simple blending or in situ chemical polymerization and electropolymerization approaches.[27−29] Visy and co-workers have illustrated the particularly noteworthy construction of magnetite/polypyrrole hybrids via the galvanostatic electrodeposition of pyrrole onto 12 nm diameter Fe_3O_4 nanoparticles prepared by alkaline hydrolysis.[30] The prepared hybrid structures show excellent photocatalytically triggered electroactivity for reduction of dissolved peroxide or oxygen.[30] Although these methods provide facile and efficacious means to engineer material properties (for example, enhanced cyclability, electrical conductivity, and reversible storage capacity for γ-Fe_2O_3 electrodes or improved barrier properties and passivation of low carbon steel for nanoparticulate Fe_3O_4 and α-Fe_2O_3/pyrrole nanocomposites),[28,29] the polydispersity of the inorganic components used thus far precludes the creation of well-ordered nanoscale polymeric arrays.

2. EXPERIMENTAL SECTION

Growth of Fe_2O_3 Nanowires. Cold-rolled steel substrates from Tata Steel with a thickness of 0.67 mm and nominal impurity content of 0.1% C, 1.5% Mn, 0.2% Si, 40 ppm N, 0.01% P, 0.002% S, 0.003% Ti were chosen for the investigation.

Initially, a simple oxidation process was used to grow α-Fe_2O_3 nanowires as per:

$$4Fe_{(s)} + 3O_{2(g)} \rightarrow 2Fe_2O_{3(s)} \quad (1)$$

The steel substrates were placed at the center of a 1″ diameter quartz tube within a tube furnace and heated to temperatures ranging from 800−1000 °C under a controlled pressure environment $<1 \times 10^{-3}$ Torr (evacuated using a mechanical pump). Subsequently, an Ar/O_2 gas mixture was flowed over the substrates at flow rates of 50−110 sccm using a gas flow proportionator (Matheson TriGas) for 1−2 h.

Growth of Polypyrrole Nanotubes. The α-Fe_2O_3 nanowires grown on the steel substrate were used as sacrificial templates for the electropolymerization of pyrrole. Initially, the oxidized steel substrate with the array of α-Fe_2O_3 nanowires was used as the working electrode and mounted in a homemade electrochemical cell at a separation of 2 mm from a cold-rolled steel counter electrode. The electrode assembly was attached to a TL0.01 dip coater (MTI Corp.) for electrode insertion and removal within the polymerization solution (0.01−0.5 M of freshly distilled pyrrole in CH_2Cl_2 or acetonitrile (J. T. Baker)) Sulfonated pyrrole was electropolymerized from an aqueous solution. Oxalate solution was used as the counterion. Electropolymerization of pyrrole was performed in galvanostatic mode at a constant current density of 2.0 mA cm^{-2} using a Keithley 220 programmable current source for 480 s at ambient temperature (25 °C). The applied current density noted here has been calculated by simply considering the geometric area of the electrode; the electrochemically active surface area is expected to be much greater given the high surface area of the α-Fe_2O_3 nanowire arrays, implying a smaller actual local current at the electrode surface. Subsequently, removal of the α-Fe_2O_3 nanowire template was performed by applying a constant current of 5 mA cm^{-2} for 2 h to the working electrode while submerged in a 30% aq. solution of H_3PO_4 (Fisher Scientific).

Characterization. The α-Fe_2O_3 nanowires were examined by using X-ray diffraction (XRD) on a Rigaku Ultima IV diffractometer with Cu Kα radiation (λ = 1.5418 Å). The operating voltage and current were maintained at 40 kV and 44 mA, respectively.

The dimensions, morphology, and elemental composition of the as-synthesized nanostructures were examined by means of scanning electron microscopy (SEM) using a Hitachi SU-70 scanning electron microscope operating at an accelerating voltage of 20 kV. For examination of the polymeric nanostructures, a carbon layer was sputtered onto the samples prior to imaging. A JEOL 2010 instrument operated at 200 kV was used to acquire high-resolution transmission electron microscopy (HRTEM) images.

Raman microprobe analysis was performed on a Jobin Yvon Horiba Labram HR instrument using a laser excitation of 514.5 nm. Fourier transform infrared (FTIR) analysis of pressed KBr pellets was performed on a ThermoNicolet instrument in transmission mode.

NEXAFS measurements were acquired on NIST beamline U7A of the National Synchrotron Light Source of Brookhaven National Laboratory at the C K-edge and the N K-edge in partial electron yield mode. NEXAFS spectra were collected in partial electron yield (PEY) mode with a channeltron electron multiplier detector near the sample surface. An electron charge compensation gun was used to eliminate charging effects for the insulating samples. To eliminate the effect of incident beam intensity fluctuations and beamline optics absorption features, the PEY signals were normalized using the incident beam intensity obtained from the photoemission yield of a freshly evaporated Au grid with 90% transmittance placed along the path of the incident X-rays. A carbon mesh was used for energy calibration of the C K-edge spectra using the π^* transition of graphite at 285.1 eV. Pre- and postedge normalization of the data was performed using the Athena and Igor suite of programs.

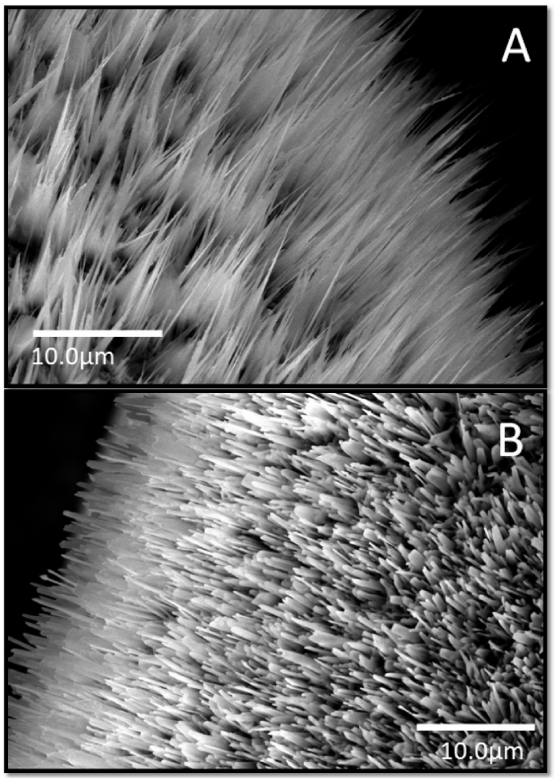

Figure 1. Scanning electron microscopy (SEM) images of vertically aligned α-Fe_2O_3 nanowire arrays grown on the low-carbon steel substrate.

3. RESULTS AND DISCUSSION

The first step of our process involves the simple high-temperature oxidation of the low carbon steel substrate at temperatures between 800 and 1000 °C and dramatically yields large-area ordered arrays of α-Fe_2O_3 nanowires as depicted in Figures 1 and 2. The scanning electron microscopy (SEM) images in Figure 1 show the uniform coverage of the nanowire forests on the low carbon steel substrate across hundreds of micrometers. Most of the nanowires evolve to a sharp and pointed tip, such as indicated in the inset to Figure 2A. The base of the nanowires is ∼40—70 nm in diameter and the pointed tips are typically <10 nm in diameter. The high-resolution transmission electron microscopy image in Figure 2B and the selected area electron diffraction pattern depicted in the inset to Figure 2B suggest that the nanowires are single crystalline along their length with the rhombohedral crystal structure of α-Fe_2O_3 and are preferentially grown along the [110] direction (Figure 2B). Figure 2C shows an X-ray diffraction pattern acquired for harvested nanowires that can be indexed to α-Fe_2O_3, hematite (JCPDS (Joint Committee on Powder Diffraction Standards) # 87−1166).

Nasibulin and co-workers have recently reported the fabrication of α-Fe_2O_3 nanowires with analogous blade-like morphologies and pointed tips grown along the [110] direction via the resistive heating of Fe wire substrates.[31] They have ascribed the growth mechanism to the rapid diffusion of Fe ions from the core of the wire through grain boundaries on oxidized FeO and Fe_3O_4 surfaces (along with the reverse diffusion of oxygen). A combination of surface diffusion along the incipient nanowires and diffusion across lattice defects such as dislocations and grain boundaries likely leads to the observed accelerated anisotropic growth.[31] The tapering of our nanowires that originally have wide blade-like bases to form pointed tips supports the manifestation of a diffusion-limited driving force for nanowire growth. In other words, at longer distances from the low carbon steel base, corresponding to longer diffusion path lengths, the supply of Fe precursors is depleted and a pronounced tapering of the nanowires is observed. An analogous "tip-growth" mechanism has also been reported by Wang and co-workers and invokes the reduction of the energy barrier for nucleation of nanowire growth owing to the presence of impurities (such as Mn, C, and Ti present in our sample).[32,33] These authors also report the formation of a graded composition of oxides on the Fe foil surface; surface diffusion of Fe ions from the core through these subsurface layers provides a steady supply of the "precursor Fe clusters" for nanowire nucleation and growth. Factors that accelerate Fe diffusion such as the presence of dopants further promote anisotropic growth.[32,33] The preferential growth along the [110] direction is explicable based on surface energy considerations taking into account the oxygen-rich nature of the resulting surfaces (as compared to more reactive Fe-rich surfaces) and the limited mobility of diffusive Fe precursors.[31,33] Consistent with this model, Raman microprobe analysis suggests the presence of characteristic α-hematite bands labeled in Figure 2D with the appropriate symmetry designations.[34]

The prepared arrays of α-Fe_2O_3 nanowires on low carbon steel are used as templates for electropolymerization of pyrrole. Electropolymerization has been performed in galvanostatic mode to ensure a constant deposition rate.[1] As suggested by Lee and co-workers, the precise mode of polymer growth along the walls of inorganic lattices depends substantially on the specifics of the growth conditions such as the applied current and monomer concentration.[3] At the high deposition currents used in our experiments, when the monomer concentration is low, on the order of 10 mM, transport of the monomer to the base electrode is diffusion limited. Consequently, polymerization is initiated along the length of the nanowires. In particular, the tapered tips and additional kinks on the nanowires likely present localized high potentials and are particularly amenable to serve as sites for nucleation and growth of polypyrrole. The SEM images in Figure 3 indicate either the patchy deposition of polypyrrole along the sidewalls of the α-Fe_2O_3 nanowires (Figure 3A, B) or the preferential deposition of polypyrrole onto the nanowire tips where the deposited polymer indiscriminately spans the tips of several nanowires (Figure 3C).

At higher monomer concentrations, sufficient local concentrations of the monomer are achieved in proximity to the base electrode and the polypyrrole layers appear to grow from the base electrode, providing more conformal coverage of the nanowires. Figure 4 depicts SEM images of polypyrrole-coated nanowires grown in galvanostatic mode at a monomer concentration of 50 mM. Notably, the nanowires are conformally coated with the polymer irrespective of their angle with respect to the base substrate.

Figures 5A and B present analogous data for a monomer concentration of 100 mM in CH_2Cl_2. At a deposition time of ∼480 s, the tapered tips of the nanowires remain free of the polymer coating, as depicted in Figure 5B. Because locally enhanced potentials are likely at the nanowire tips, the morphology of the polymer coating observed in Figure 5B corroborates the idea of base growth of polypyrrole from the flat underlying steel electrode.[3] Remarkably, upon electrochemically etching the α-Fe_2O_3 nanowires with H_3PO_4, the dissolution of the nanowires leaves behind arrays of polypyrrole nanotubes that substantially capture the faceted geometry of the nanowire templates (Figure 5C, D).

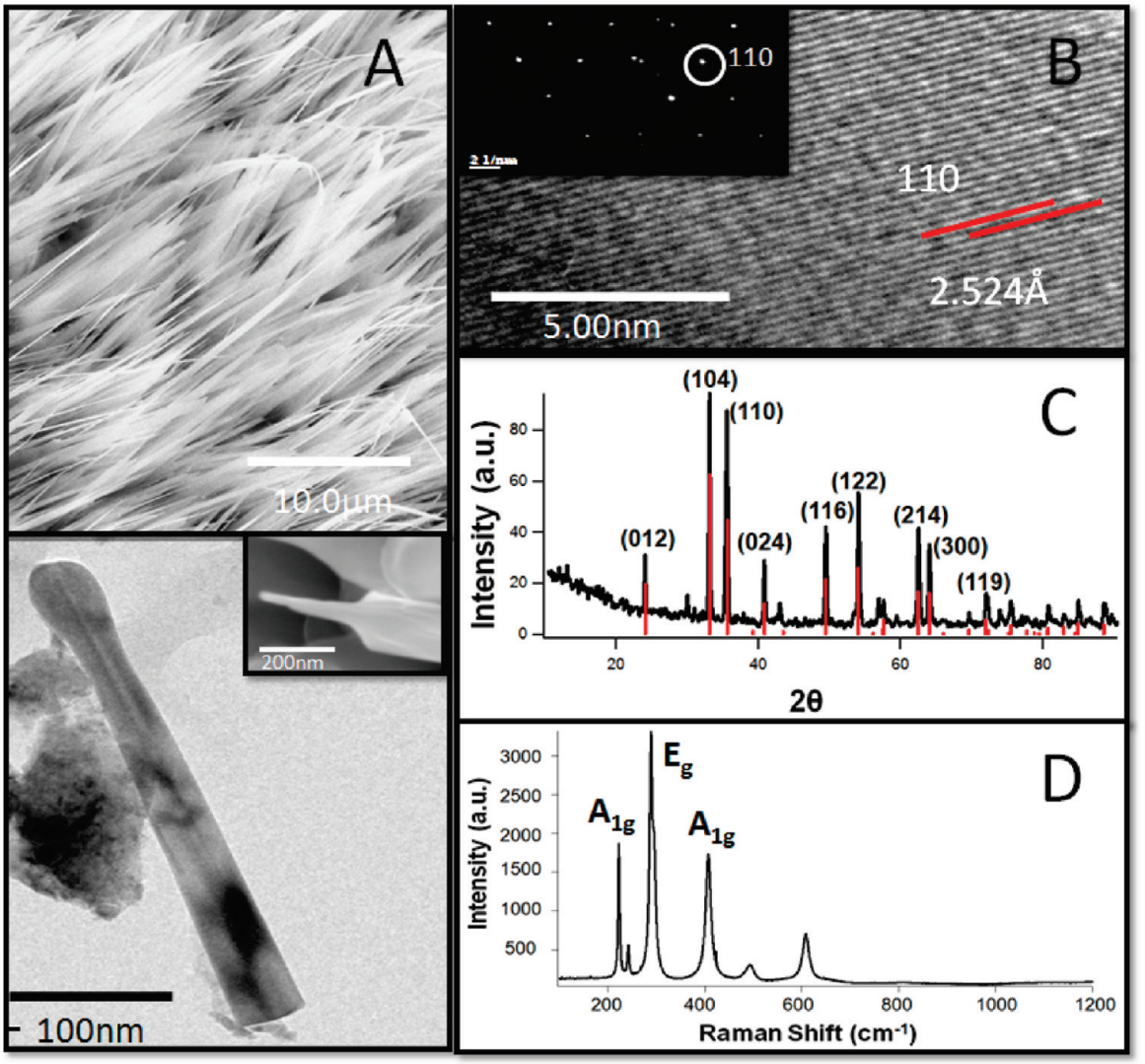

Figure 2. (A) High-resolution SEM and transmission electron microscopy (TEM) images of α-Fe_2O_3 nanowires; the inset shows a tapered faceted tip, as is characteristically observed for nanowires obtained via our low carbon steel substrate process. (B) HRTEM lattice-resolved image of a single nanowire showing the separation between (110) planes; the inset shows the selected area electron diffraction (SAED) pattern acquired at the same region. (C) Indexed X-ray diffraction pattern of α-Fe_2O_3 nanowire arrays. (D) Raman spectrum acquired for α-Fe_2O_3 nanowire arrays.

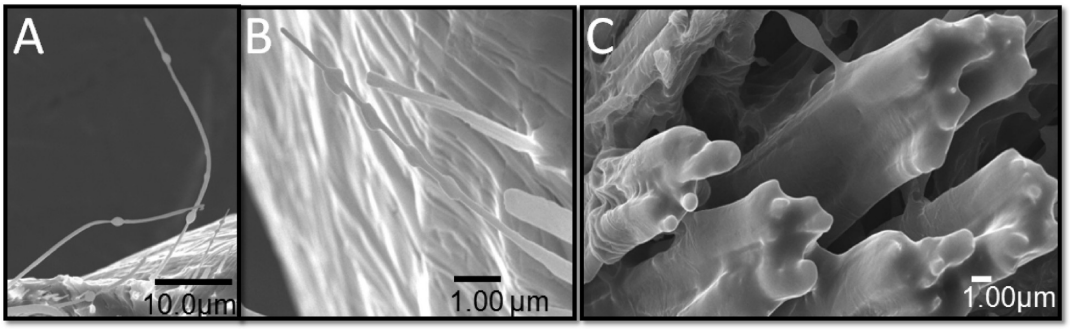

Figure 3. (A, B) SEM images illustrate the patchy deposition of polypyrrole to form bulbous regions along the sidewalls or (C) the preferential deposition of polypyrrole across α-Fe_2O_3 nanowire tips obtained at a monomer concentration of 0.01 M .

At still higher monomer concentrations on the order of 500 mM, rapid electropolymerization leads to substantial aggregation of polymer-coated nanowires, and indeed instead of individual nanowires, clumps of nanowires are noted to be coated with polypyrrole (Figure 6A). Fast and uncontrolled polymerization also starts to lead to the growth of macroscopic granules of

polypyrrole on the nanowire surfaces (Figure 6B). In analogy with observations for growth of polypyrrole nanotubes and nanowires within templates, optimization of the monomer concentration is of paramount importance to control the initiation and growth dynamics of polypyrrole electropolymerization.[1,3,5,7] On a related note, the simultaneous optimization of the current density is also critical for control of deposition of well-defined polypyrrole nanostructures with conformal coverage on the underlying nanowire substrates. For the concentrations screened here, current densities lower than 2 mA/cm^2 (based on the geometrical electrode area as noted above) gives patchy coverage; lowering the current density to less than 1 mA/cm^2 does not yield visibly discernible polypyrrole films.

Anodic oxidation of the monomers at the electrode likely leads to formation of soluble oligomers that rapidly saturate the interstitial spaces between the nanowires on the substrate.[1] Upon interfacial saturation, instantaneous nucleation and growth begins either at the base electrode or directly on the nanowires depending upon the monomer concentration. Subsequently, further cross-linking of the incipient polymers leads to the growth of robust polymeric architectures that survive the electrochemical etching of the Fe_2O_3 nanowires.

Figure 7A shows FTIR data acquired for the polypyrrole nanotubes. The 3000−3600 cm^{-1} region is characterized by the distinctive presence of N−H bonds. A band observed at 1638 cm^{-1} can be attributed to C═C stretching modes (also possibly C═O groups formed by overoxidation of polypyrrole), whereas peaks at 1558 and 1473 cm^{-1} correspond to pyrrole ring stretching and C−N stretching vibrations, respectively.[35] Analogously, features at 756 and 619 cm^{-1} can be ascribed to out-of-plane C−H and N−H deformations, respectively.[35]

Figures 7B and C show angle-resolved C K-edge and N K-edge NEXAFS data. The prominent feature at ~285.5 eV observed in the C K-edge spectra can be ascribed to π^* resonance derived from transitions of 1*s* electrons to the unoccupied counterparts of −C═C− bonding orbitals above the Fermi level.[36,37] Note that bipolaronic features are not expected to be observed at the beam fluxes used in these experiments[37] but the prominent π^* feature nevertheless attests to the conjugated nature of the prepared polymeric nanostructures. The intensity of the π^* feature does not show any discernible angle-dependence suggesting that the

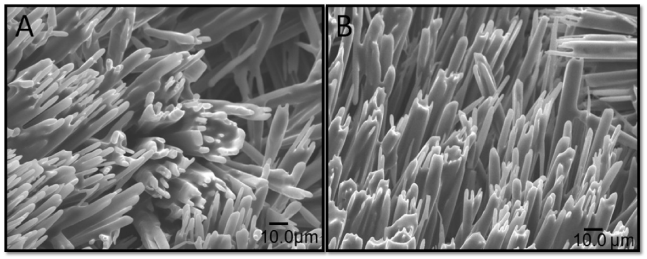

Figure 4. (A, B) SEM images of polypyrrole-coated nanowires obtained at a monomer concentration of 0.05 M.

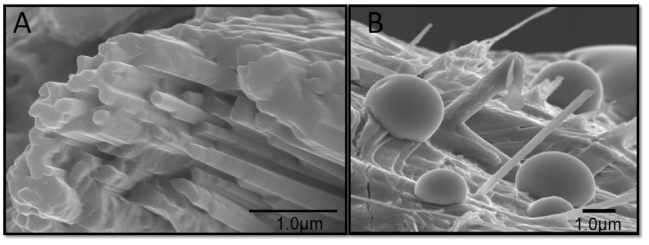

Figure 6. (A, B) SEM of α-Fe_2O_3 nanowires polymerized at higher monomer concentrations on the order of 0.5 M.

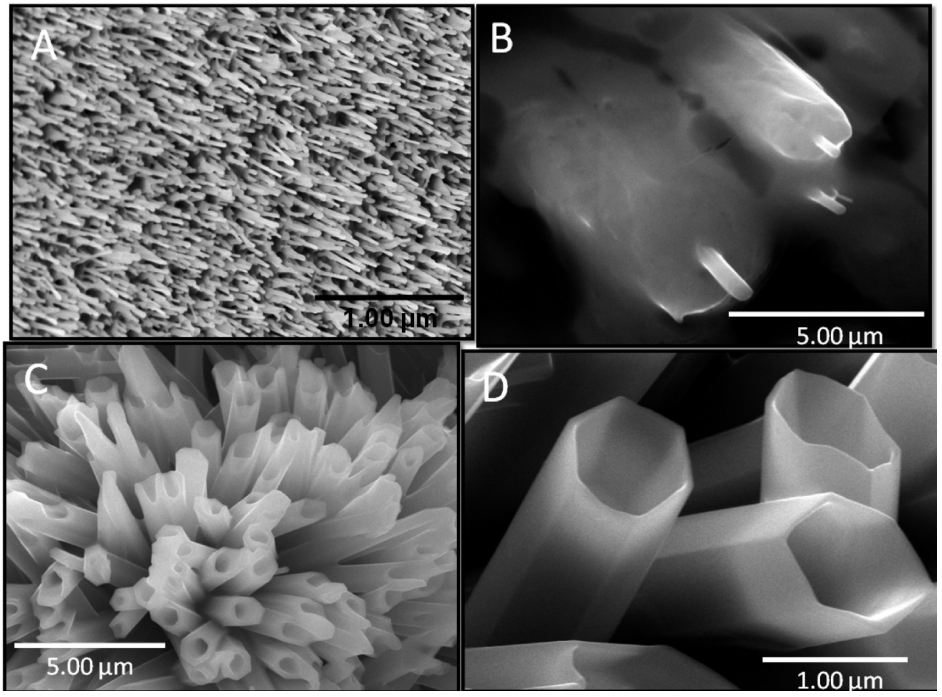

Figure 5. SEM images illustrating the electropolymerization performed at a monomer concentration of 0.1 M: (A) α-Fe_2O_3 nanowire array coated with polypyrrole; (B) high-magnification SEM image of the electropolymerization of a single α-Fe_2O_3 nanowire; (C) overview SEM image of an array of polypyrrole nanotubes; and (D) high-magnification SEM image of polypyrrole nanotubes.

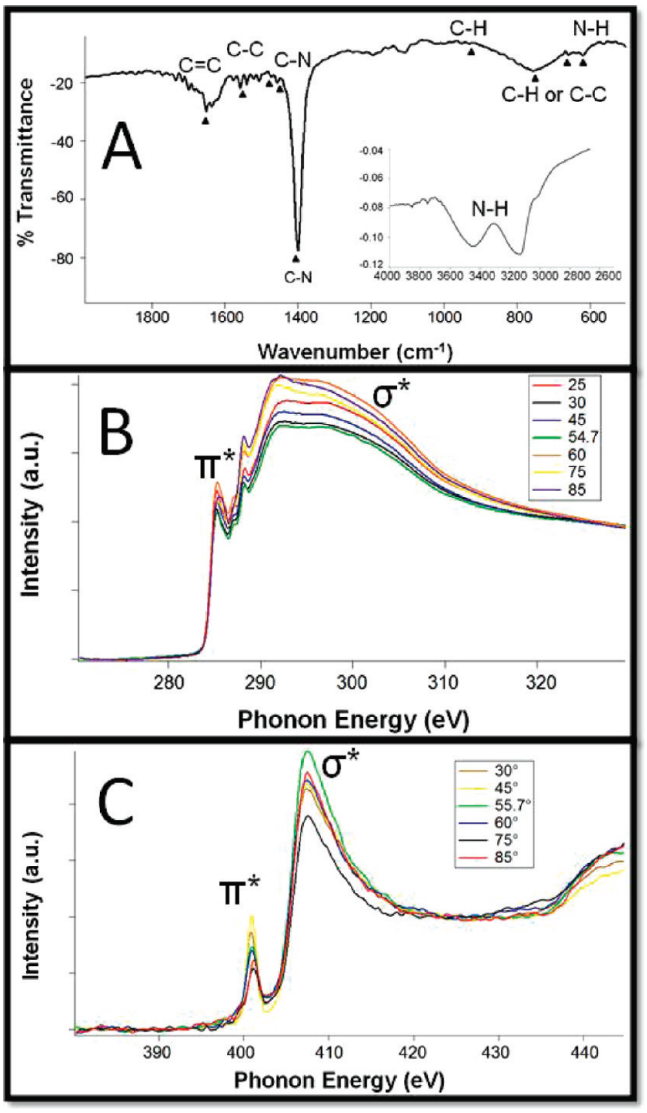

Figure 7. (A) FTIR spectra of polypyrrole nanotubes; (B) NEXAFS data acquired at the C-Kedge, transitions of 1*s* electrons to the unoccupied counterparts of −C═C− bonding orbitals; (C) N-Kedge illustrate the significantly weaker π^* feature compared to the σ^* feature, characteristic of polypyrrole.

polypyrrole nanostructures are completely amorphous despite their occasionally faceted appearance. Martin and co-workers (among others) have observed an increased conjugation length and structural ordering of polymer chains for the first deposited polymer layer within the pores of alumina membranes.[7] However, this ordering is rapidly lost upon the deposition of subsequent layers wherein the polymer chains adopt random conformations. The 287−290 regions have a couple of distinctive features that can be attributed to transitions from C 1*s* states to partially filled and unoccupied states derived primarily from C−H* and C−N* antibonding interactions.[36,37] The higher energy features above 288 eV correspond to transitions to C−C and C═C σ^* states. Extended conjugation is also evidenced by the pronounced asymmetric π^* feature noted at the N K-edge (Figure 7C).[37,38] Again, no discernible angle-dependence of the intensity of this feature has been observed further corroborating the completely amorphous and random arrangement of polymer chains within the polymeric nanostructures. Notably, the π^* feature is significantly weaker than the σ^* feature, as is characteristic of polypyrrole (the reverse order of intensities is observed for the pyrrole monomer).[38] Pavlychev and co-workers have noted that upon polymerization the electron density delocalized over the C−N bond in pyrrole becomes more localized on the N atom (since the C atom is also involved in bonding to the adjacent pyrrole unit). The redistribution of electron occupancies results in a diminution of the π^* feature upon polymerization as is indeed observed for our nanostructures.[38] The cyclic voltammagrams in Figure S1 (Supporting Information) confirm the electroactivity of the polypyrrole nanotube film and is compared to a polypyrrole film galvanostatically deposited on a flat carbon steel substrate. Future work will focus on optimization of the electroactivity of the prepared nanotubes through judicious choice of the counterion and electrolyte.

The electropolymerization and electrochemical etching procedure described here should in principle be generalizable to all conjugated polymers that can be anodically electropolymerized.[1,2,4] Figure S2 (Supporting Information) shows a limited set of data acquired for functionalized polypyrrole nanostructures fabricated by the galvanostatic electropolymerization of self-doped sulfonated polypyrrole in aqueous media. Scheme S1 (Supporting Information) shows the structure of sulfonated pyrrole used as the monomer in this process.

4. CONCLUSIONS

The set of processes described here based on simple oxidation of low carbon steel to generate α-Fe_2O_3 nanowire arrays, followed by electropolymerization of pyrrole onto the nanowires, and electrochemical phosphoric acid etching of the inorganic cores provides for a facile and inexpensive means for generating polymeric nanostructures and will have great practical utility for the large-scale fabrication of polymeric nanostructures. Core-shell Fe_2O_3/polypyrrole nanocomposite coatings may also prospectively be important in their own right for corrosion protection or as composite electrodes for electrochemical double layer capacitors and Li-ion batteries.[28,29] The simple approach described here should be broadly generalizable to functionalized pyrroles and other electropolymerizable heteroaromatic monomers.

■ ASSOCIATED CONTENT

Ⓢ Supporting Information. Cyclic voltammagrams of polypyrrole nanotubes. Chemical structure of the sulfonated pyrrole monomer along with SEM images and FTIR data of sulfonated polypyrrole nanotubes (PDF). This material is available free of charge via the Internet at http://pubs.acs.org/.

■ AUTHOR INFORMATION

Corresponding Author

*E-mail: tapan-kumar.rout@tatasteel.com (T.K.R.); jrzayev@buffalo.edu (J.R.); sb244@buffalo.edu (S.B.).

■ ACKNOWLEDGMENT

Nidya Dewi and Theodore Glave are acknowledged for preliminary experimental assistance. This work was primarily supported by the Tata Steel Group. S.B. acknowledges partial support of this work from the National Science Foundation

under DMR 0847169. J.M.V. is grateful to NASA for a Harriet G. Jenkins graduate fellowship.

REFERENCES

(1) Heinze, J.; Frontana-Uribe, B. A.; Ludwigs, S. *Chem. Rev.* **2010**, *110*, 4724–4771.
(2) Malinauskas, A.; Malinauskene, J.; Ramanavicius, A. *Nanotechnology* **2005**, *16*, R51–R62.
(3) Cho, S.-I.; Lee, S. B. *Acc. Chem. Res.* **2008**, *41*, 699–707.
(4) Pan, L.; Qiu, H.; Dou, C.; Li, Y.; Pu, L.; Xu, J.; Shi, Y. *Int. J. Mol. Sci.* **2010**, *11*, 2636–2657.
(5) Jerome, C.; Demoustier-Champagne, S.; Legras, R.; Jerome, R. *Chem.—Eur. J.* **2000**, *6*, 3089–3093.
(6) Martin, C. R. *Science* **1994**, *266*, 1961–1966.
(7) Martin, C. R. *Chem. Mater.* **1996**, *8*, 1739–1746.
(8) Lee, J. I.; Cho, S. H.; Park, S.-M.; Kim, J. K.; Kim, J. K.; Yu, J.-W.; Kim, Y. C.; Russell, T. P. *Nano Lett.* **2008**, *8*, 2315–2320.
(9) Jang, J.; Oh, J. H. *Chem. Commun.* **2004**, *2004*, 882–883.
(10) Lahav, M.; Weiss, E. A.; Xu, Q. B.; Whitesides, G. M. *Nano Lett.* **2006**, *6*, 2166–2171.
(11) Chen, J. H.; Huang, Z. P.; Wang, D. Z.; Yang, S. X.; Li, W. Z.; Wen, J. G.; Ren, Z. F. *Synth. Met.* **2002**, *125*, 289–294.
(12) *Handbook of Conducting Polymers*, 3rd ed.; Skotheim, T. A.; Reynolds, J. R., Eds.; CRC Press: Boca Raton, FL, 2007.
(13) Inzelt, G. *Conducting Polymers*; Springer: Heidelberg, 2008.
(14) Hughes, M.; Chen, G. Z.; Shaffer, M. S. P.; Fray, D. J.; Windle, A. H. *Chem. Mater.* **2002**, *14*, 1610–1613.
(15) Wang, Y. G.; Li, H. Q.; Xia, Y. Y. *Adv. Mater.* **2006**, *18*, 2619–2623.
(16) Liu, R.; Lee, S. B. *J. Am. Chem. Soc.* **2008**, *130*, 2942–2943.
(17) Jang, J.; Oh, J. H.; Stucky, G. D. *Angew. Chem., Int. Ed.* **2002**, *41*, 4016–4019.
(18) Jang, J.; Yoon, H. *Chem. Commun.* **2003**, *6*, 720–721.
(19) Jang, H.; Yoon, H. *Langmuir* **2005**, *21*, 11484–11489.
(20) Hatano, T.; Bae, A.-H.; Takeuchi, M.; Fujita, N.; Kaneko, K.; Ihara, H.; Takafuji, M.; Shinkai, S. *Angew. Chem., Int. Ed.* **2004**, *43*, 465–469.
(21) Shi, W.; Ge, D.; Wang, J.; Jiang, Z.; Ren, L.; Zhang, Q. *Macromol. Rapid Commun.* **2006**, 27.
(22) Shi, W.; Liang, P.; Ge, D.; Wang, J.; Zhang, Q. *Chem. Commun.* **2007**, 2414.
(23) Huang, K.; Canterbury, D. P.; Rzayev, J. *Chem. Commun.* **2010**, *46*, 6326–6328.
(24) Wang, D.; Liu, Y.; Wang, C.; Zhou, F.; Liu, W. *ACS Nano* **2009**, *3*, 1249–1257.
(25) Zhang, X.; Manohar, S. K. *J. Am. Chem. Soc.* **2004**, *126*, 12714–12715.
(26) Zhang, X.; Manohar, S. K. *J. Am. Chem. Soc.* **2005**, *17*, 14156–14157.
(27) Zhang, P.; Zhang, Z. H.; Wang, D. J.; Kan, S. H.; Chai, X. D.; Liu, J. Z.; Li, T. J. *Synth. Met.* **1997**, *84*, 165–166.
(28) Kwon, C.-W.; Poquet, A.; Mornet, S.; Campet, G.; Portier, J.; Choy, J.-H. *Electrochem. Commun.* **2002**, *4*, 197–200.
(29) Garcia, B.; Lamzoudi, A.; Pillier, F.; Nguyen Thi Le, H.; Deslouis, C. *J. Electrochem. Soc.* **2002**, *149*, B560–B566.
(30) Janaky, C.; Endrodi, B.; Berkesi, O.; Visy, C. *J. Phys. Chem. C* **2010**, *114*, 19338–19344.
(31) Nasibulin, A. G.; Rackauskas, S.; Jiang, H.; Tian, Y.; Mudimela, P. R.; Shandakov, S. D.; Nasibulina, L. I.; Sainio, J.; Kauppinen, E. I. *Nano Res.* **2009**, *2*, 373–379.
(32) Chueh, Y.-L.; Lai, M.-W.; Liang, J.-Q.; Chou, L.-J.; Wang, Z. L. *Adv. Funct. Mater.* **2006**, *16*, 2243–2251.
(33) Wen, X.; Wang, S.; Ding, Y.; Wang, Z. L.; Yang, S. H. *J. Phys. Chem. B* **2005**, *109*, 215–220.
(34) de Faria, D. L. A.; Lopes, F. N. *Vib. Spectrosc.* **2007**, *45*, 117–121.
(35) Omastova, M.; Trchova, M.; Kovarova, J.; Stejskal, J. *Synth. Met.* **2003**, *138*, 447–455.
(36) Yang, X. Q.; Chen, J.; Hale, P. D.; Inagaki, T.; Skotheim, T. A.; Fischer, D. A.; Okamoto, Y.; Samuelson, L.; Tripathy, S.; Hong, K.; Watanabe, I.; Rubner, M. F.; den Boer, M. L. *Langmuir* **1989**, *5*, 1288–1292.
(37) Kappen, P.; Hale, P. S.; Brack, N.; Prissanaroon, W.; Pigram, P. J. *Appl. Surf. Sci.* **2006**, *253*, 1473–1479.
(38) Pavlychev, A. A.; Hallmeier, K. H.; Hennig, C.; Henning, L.; Szargan, R. *Chem. Phys.* **1995**, *201*, 547–555.